Dalton Transactions

An international journal of inorganic chemistry

Accepted Manuscript

This article can be cited before page numbers have been issued, to do this please use: C. Evangelisti, W. Oberhauser, F. Poggialini, E. Pitzalis, T. X. Nguyen, E. Punzi, S. Coiai, N. Scotti, L. Poggini and A. Mandoli, *Dalton Trans.*, 2026, DOI: 10.1039/D5DT02604K.

This is an Accepted Manuscript, which has been through the Royal Society of Chemistry peer review process and has been accepted for publication.

Accepted Manuscripts are published online shortly after acceptance, before technical editing, formatting and proof reading. Using this free service, authors can make their results available to the community, in citable form, before we publish the edited article. We will replace this Accepted Manuscript with the edited and formatted Advance Article as soon as it is available.

You can find more information about Accepted Manuscripts in the Information for Authors.

Please note that technical editing may introduce minor changes to the text and/or graphics, which may alter content. The journal's standard Terms & Conditions and the Ethical guidelines still apply. In no event shall the Royal Society of Chemistry be held responsible for any errors or omissions in this Accepted Manuscript or any consequences arising from the use of any information it contains.

ROYAL SOCIETY OF CHEMISTRY

rsc.li/dalton

View Article Online
DOI: 10.1039/D5DT02604K

Covalent triazine framework @ silica core-shell spheres decorated with ultrafine platinum nanoparticles: a robust catalyst for selective aqueous phase hydrogenation of butane-2,3-dione and pyruvic acid

Claudio Evangelisti,*[a] Werner Oberhauser,*[b] Francesco Poggialini,[a] Emanuela Pitzalis,[a] Xuan Trung Nguyen,[a] Esther Punzi,[a] Serena Coiai,[a] Nicola Scotti,[c] Lorenzo Poggini,[b,d] and Alessandro Mandoli[e]

[a] *Institute of Chemistry of OrganoMetallic Compounds, ICCOM-CNR, Via G. Moruzzi 1, 56124 Pisa, Italy.*

[b] *Institute of Chemistry of OrganoMetallic Compounds, ICCOM-CNR, Via Madonna del Piano 10, 50019 Sesto Fiorentino, (FI), Italy.*

[c] *Institute of Science and Chemical Technologies "Giulio Natta", SCITEC-CNR, Via C. Golgi 19, 20133 Milano, Italy.*

[d] *Department of Chemistry "U. Schiff" - DICUS – and INSTM Research Unit, University of Florence, Via della Lastruccia 3-13, 50019 Sesto Fiorentino (FI), Italy.*

[e] *Department of Chemistry and Industrial Chemistry, University of Pisa, Via G. Moruzzi 13, 56124 Pisa, Italy.*

View Article Online
DOI: 10.1039/D5DT02604K

Abstract

Sub-nanometric sized Pt nanoparticles, generated by metal vapor synthesis technique, were supported onto covalent triazine framework @ silica (CTF@SiO_2) core-shell hybrid microspheres obtained through polycondensation reactions at the SiO_2 surface. The later catalyst and a reference system (*i.e.* Pt nanoparticles deposited onto bare SiO_2 microspheres) were screened under identical experimental conditions in the hydrogenation of butane-2,3-dione and pyruvic acid in water, leading to butane-2,3-diol and lactic acid in high selectivity. A combination of catalytic recycling experiments was conducted with both catalysts, along with transmission electron microscopy and X-ray diffraction analyses performed on either as-synthesized and recovered catalysts confirmed the remarkable role of the CTF shell layer on the stabilization of ultrafine Pt NPs against their aggregation under catalysis as well as on its catalytic activity.

KEYWORDS: Platinum / Covalent Triazine Framework / Hydrogenation / Butane-2,3-dione / Pyruvic Acid

View Article Online
DOI: 10.1039/D5DT02604K

1. Introduction

Since their first report in 2005, covalent organic frameworks (COFs) have received an increasing interest in catalysis.[1,2] The ordered structure and the light element composition of COFs-based materials lead to high specific surface area and adjustable pore sizes. Moreover, their customizable structure allows for various functional groups, making them promising materials for different catalytic applications such as photocatalysis, electrocatalysis, energy storage, and fine chemical production.[1,3,4] Among COFs, covalent triazine frameworks (CTFs) stand out due to their unique porous structure, which is attributed to the 1,3,5-triazine units with π-conjugation properties that enhance their thermal and chemical stability.[5-7] Their high nitrogen content, high surface area, and high porosity make them versatile hosts for catalytically active metal species, ranging from single metal atoms to nanoparticles (NPs).[8-9] In fact, porosity of the polymeric support layer along with a favourable electron donor property of the support is a prerequisite for high catalytic activity in metal-based heterogeneous catalysis.[10-12] Recently, both noble and non-noble metal NPs like Pd, Pt and Ni [13-15] have been successfully immobilized on CTFs, exhibiting elevated dispersion even at high metal loadings and improved catalytic efficiency and recyclability/durability for selective hydrogenation reactions with respect to conventional supports (*e.g.* carbon).

Although different synthesis approaches for CTFs have been developed,[16] the large-scale production of these materials remains still a challenge up to now.[17]

Hybrid particles with a silica core and a CTF porous shell combine the advantages of the shell material and the mechanical stability of silica, significantly reducing the required amount of CTF material. As a consequence, the synthesis of the catalytic support can easily be scaled up. In this work, we present a facile approach to fabricate morphology-controllable CTFs shell through polycondensation reactions using SiO_2 core spheres as a hard template. Sub-nanometer Pt NPs were generated by metal vapour synthesis (MVS),[18,19] which allow the synthesis of size-tailored metal NPs regardless of the support nature. The CTF@SiO_2 system was selected as carrier for the ultrafine Pt NPs to get the Pt/CTF@SiO_2 composite (**1**). Pure silica spheres were also used to obtain the Pt/SiO_2 system (**2**) as a

View Article Online
DOI: 10.1039/D5DT02604K

reference catalytic material. Both latter heterogeneous catalysts were thoroughly characterized by microscopic, spectroscopic, diffraction and thermogravimetric techniques and then used to promote the hydrogenation of butane-2,3-dione (2,3-BDO) and of pyruvic acid (PyA) in water. The chemo-selective conversion of both substrates into butane-2,3-diol and lactic acid, respectively, which are known to be bio-based platform molecules[20,21] is challenging, since either substrate undergo undesired side reactions due to their reactivity (*i.e.* dimerization of 2,3-BDO due to the keto-enol tautomerization[22] and decarboxylation of PyA[23]). Hence the development of an efficient, recyclable hydrogenation catalyst, which is efficiently operative at relatively low reaction temperature to prevent high temperature-stirred side reactions would be highly welcome. To this aim, we propose a heterogeneous nitrogen-atom stabilizing support material that efficiently stabilizes Pt NPs and Pt-N interactions occurring at the interface foster heterolytic hydrogen splitting, which is ideal for polar functional group hydrogenation.[24,25]

2. Experimental

2.1 Materials

Mesitylene (98 %, Merck®) was distilled over metallic Na and then stored in a dry argon atmosphere. The following reagents were purchased from Merck® and used as received without any further purification: ethanol (purity 99.0 %), ammonia solution (25-28 %), tetraethoxysilane (TEOS, purity 98.0 %), (3-aminopropyl) triethoxysilane (APTES, purity 99.0 %), dimethyl sulfoxide (purity 99.7 %), terephthalaldehyde (TPA, purity 99.0 %), cesium carbonate (purity 99.0 %), tetrahydrofurane (THF, purity 99.9 % inhibitor free), *n*-pentane (purity 99.0 %). 2,3-BDO and PyA were purchased from Aldrich and used as received. Water used for catalytic reactions was bidistilled prior to use.

View Article Online
DOI: 10.1039/D5DT02604K

2.2 Synthesis

Synthesis of SiO_2 spheres

Deionized water (40 mL) and ethanol (240 mL) were mixed at 32 °C for 30 min, then ammonia solution (6.8 mL) was slowly added to the latter mixture. Afterwards, TEOS (24 mL) was quickly added to the solution and reaction continued for 5 h, giving monodisperse SiO_2 nanospheres, which were washed several times with ethanol, centrifuged and then vacuum dried for 24 h.

Synthesis of CTF@SiO_2

The covalent triazine framework grafted on silica nanospheres (CTF@SiO_2) was synthesized following a previously reported procedure.[26] SiO_2 nanospheres (5.0 g) were dispersed in ethanol (900 mL) by sonication. Then, APTES (1.5 mL) and ethanol (100 mL) were mixed and then slowly added to the silica ethanol suspension under vigorous stirring at 32 °C. The reaction continued for 12 h yielding an amino group-functionalized silica (NH_2-SiO_2), which was washed with water and ethanol by centrifugation and redispersion, and dried by vacuum for 24 h. Then, NH_2-SiO_2 (625 mg) was suspended in DMSO (50 mL) and ultrasonically dispersed at ambient temperature until a uniform suspension was obtained. Afterwards, terephthalaldehyde (TPA, 8.0 mg) was added to the above suspension which was stirred at 60 °C for 12 h, followed by the addition of 1,4-terephthalamidine dihydrochloride (52.9 mg), synthesized according to ref. [27] (see SI section 1.1 for details), and cesium carbonate (120 mg) at 60°C. The reaction continued for 12 h at the latter temperature, before it was raised to 80 °C and maintained at the latter temperature for 12 h. Then terephthalaldehyde (25.5 mg), 1,4-terephthalamidine dihydrochloride (171.1 mg and cesium carbonate (240 mg) were added to the above reaction system and reacted at 100°C for 24 h. The temperature was then maintained at 120 °C for an additional 24 h. The solid (CTF@SiO_2) was washed with H_2O and centrifuged. The

obtained solid was then transferred back to the flask, stirred in THF for 2 h, centrifuged, washed again with THF and then dried by vacuum for 1 day (final mass 781 mg).

Synthesis of Pt NPs

The synthesis of sub-nanometric Pt NPs was carried out following the metal vapor synthesis (MVS) method. [18] Briefly, Pt vapor generated at 10^{-5} mbar by resistive heating was condensed with mesitylene vapor (100 mL) onto the cold walls of a glass reactor maintained at -196 °C (liquid nitrogen) for 1 h. The reactor chamber was then heated to the melting point of the solid matrix (ca. -40 °C) and the resulting mesitylene-stabilized Pt metal atoms (95.0 mL, 0.80 mg/mL Pt, measured by ICP-OES) were kept under argon atmosphere in a Schlenk tube at -80 °C.

*Synthesis of Pt/CTF@SiO_2 (**1**)*

A Pt/mes solution (20 mL) was added to CTF@SiO_2 (800 mg) dispersed in mesitylene (10.0 mL) under stirring for 12 h. Afterwards the solvent was removed and the obtained solid (Pt/CFT@SiO_2) was washed with *n*-pentane (3 x 20 mL) and dried under reduced pressure to give **1** (810 mg) as a yellow-brown powder. The Pt loading determined by ICP-OES (2.0%) indicated a nearly quantitative deposition of the metal on the support.

Synthesis of Pt/SiO_2 (2)

The synthesis of **2** was prepared by applying the same synthesis method and using SiO_2 spheres (reported in section 2.2) instead of CTF@SiO_2, as support. A quantitative deposition of Pt clusters

View Article Online
DOI: 10.1039/D5DT02604K

onto the support was obtained leading to a final Pt loading of 2.0 wt.%, as proved by ICP-OES analysis conducted on **2**.

2.3 Characterization

Inductively coupled plasma – optical emission spectroscopy (ICP-OES) analyses were carried out with an ICP-Optical emission dual view Perkin Elmer OPTIMA 8000 apparatus. The Pt/mes solution (0.5 mL) (MVS) was heated over a heating plate in a porcelain crucible to remove the solvent, and the solid residue was digested in aqua regia (2.0 mL) for 6 h. The latter solution was then diluted with ultrapure water (PureLab Pro, 18.2 MΩ.cm). For the determination of the catalysts' metal loading, the catalyst (10 mg) was treated with aqua regia (4 mL) and refluxed for 6 h. The suspension was then diluted with diluted with ultrapure water and centrifuged to remove the silica residue. Quantification of Pt was obtained by means of a calibration curve obtained with suitable diluted Pt stock solutions. The limit of detection (L.O.D.) calculated for platinum was 2 ppb. In all cases, the results of MVS solution and catalyst loading were highly consistent.

Fourier-transformed infrared (FT-IR) spectra were recorded in ATR mode on sample powder using a Frontiers FTIR spectrometer (Perkin Elmer, Milan, Italy), equipped with a diamond-attenuated total reflectance (ATR) sampling accessory. For each sample three spectra were recorded in 4000–600 cm^{-1} spectral range with a 4 cm^{-1} resolution, with 32 scans for the background and the sample.

Nitrogen physisorption isotherms were collected with a Micromeritics ASAP2020 instrument. Prior to the analysis carried out at 77 K, the sample was treated under high vacuum at 200 °C for 2 h.

Powder X-ray diffraction (PXRD) was carried out with a PANalytical powder diffractometer equipped with a copper anode (CuKα-radiation, λ = 1.541874Å) and a PIXcel detector. Samples were

View Article Online
DOI: 10.1039/D5DT02804K

prepared on a Si wafer (zero background) and spectra acquired in the 2Θ interval from 10.0 to 80.0° with a step size of 0.0263° and a counting time of 167.8 s.

Transmission Electron Microscopy (TEM) characterization was performed using a Talos™ F200X G2 TEM microscope (Thermo Scientific). Energy dispersive X-ray spectra (EDS) and element maps were collected along with HAADF-STEM (high angular annular dark field scanning transmission electron microscopy) micrographs and four-detector Super-X Energy Dispersive. Samples for analysis were ultrasonically dispersed in *iso*-propyl alcohol and a drop of the suspension was deposited on a holey carbon copper grid (300 mesh).

X-ray photoelectron spectroscopy (XPS) analyses were carried out in a UHV chamber (10^{-9}/10^{-10}mbar) equipped with non-monochromatized Al radiation (hυ = 1486.6 eV, VSW-TA1) combined with a hemispherical electron/ion energy analyzer (VSW-HA100 with a 16-channel detector). The operating power of the X-ray source was 144 W (12 kV and 12 mA), and photoelectrons were collected normal to the sample surface, maintaining the angle between the analyzer axis and the X-ray source fixed at 54.5°. All samples were adsorbed on carbon tape, and the XPS spectra were acquired in a fixed analyzer transmission mode with a pass energy of 44.0 eV. CasaXPS software was used to analyze the spectra and a linear or Shirley function was used for the background correction. The deconvolution of XPS spectra has been performed by applying a combination of Gaussian and Lorentzian functions (70/30 ratio) for N1*s* and C1*s* and Lorentzian Asymmetric Lineshapes for Al2*p* and Pt4*f*. All the binding energies (B.E.) were calibrated upon fixing C1*s* of the carbon tape at 285.1 eV.[28]

Thermogravimetric analyses (TGA) were carried out using a SEIKO SII TG/DTA 7200 EXSTAR instrument (Chiba, Japan). Samples with masses between 3 and 5 mg were heated from 30 to 900 °C under a nitrogen flow of 200 mL min^{-1}, at a constant heating rate of 10 °C min^{-1}. The rate inflection temperatures corresponding to the different degradation steps were determined from the first-derivative thermogravimetric (DTG) curves. The final residue was evaluated at 900 °C.

View Article Online
DOI: 10.1039/D5DT02604K

High performance liquid chromatography (HPLC) analyses were carried out on a HPLC apparatus (Shimadzu), equipped with an Aminex HPX-87H chromatograhic column (300 × 7.8 mm) (BIO-RAD) and a RID 10A detector. All analyses were carried out using sulfuric acid (0.005M) as eluent and applying a flow rate of 0.4 mL/min and a column temperature of 35 °C. All organic compounds were quantified by means of calibration curves.

^{1}H NMR spectra were recorded with a Bruker AVANCE 400 spectrometer at room temperature using an Evans tube filled with D_2O.

Gas chromatography-mass spectrometry (GC-MS) was carried out with a GC-MS 2010SE apparatus (Shimadzu) equipped with a capillary column (VF WAXms, 30.0 m × 0.25 mm × 0.25 μm) and He as carrier gas.

2.4 Catalysis

Catalytic hydrogenation reactions were conducted in a teflonated stainless steel autoclave (70 mL) equipped with magnetic stirring an electronic pressure controller and a thermocouple. The autoclave was heated by means of an external temperature-controlled oil bath. Typically, catalytic reactions were conducted as follows: The autoclave was charged with catalyst (20 mg) then sealed and evacuated. Afterwards a deaerated water solution of the substrate (20 mL, 57.5 mM) was introduced into the autoclave by suction, followed by heating it to the desired temperature. Once the reaction temperature was reached, the autoclave was pressurized with hydrogen (25 bar) and magnetically stirred for the desired reaction time. The autoclave was then cooled to 10 °C by means of a water-ice bath, excess gas vented off and the solid catalyst separated from water solution by centrifugation. The clear water solution was analysed by HPLC, ^{1}H NMR spectroscopy, GC-MS spectrometry and ICP-OES. Recycling experiments were carried out upon washing the separated catalyst with water followed by centrifugation. The wet catalyst was then redispersed in water (20 mL) which contained

View Article Online
DOI: 10.1039/D5DT02604K

the substrate (1.15 mmol). The obtained suspension was transferred into the evacuated autoclave by suction. The autoclave was then successively, sealed, slowly flushed with hydrogen for 2 minutes, heated to the desired temperature and then pressurized with hydrogen (25 bar) followed by magnetically stirring of the reaction suspension. Catalysts **1** and **2**, recovered and objected to TEM, XPS and PXRD analyses were extensively rinsed with water and then vacuum-dried at 50 °C.

3. Results and discussion

3.1 Synthesis and characterization of the materials

The synthesis approach of SiO_2 spheres and CTF@SiO_2 spheres is represented in Fig. 1. Following a previously reported procedure,[27] uniform SiO_2 spheres with diameters ranging 240-260 nm were prepared. The SiO_2 spheres were treated with (3-Aminopropyl) triethoxysilane (APTES) and the amino groups present at their surface were further used to anchor terephthalaldehyde by a Schiff base reaction (see FT-IR spectra reported in Fig. S1). The aldehyde monomers were then reacted with 1,4-terephthalamidine dihydrochloride at the surface of the material and finally both precursors were added simultaneously to obtain the final CTF@SiO_2.

Ultrafine Pt NPs were synthesized as ligand-free particles in their reduced form by MVS approach[19,29] and supported on either CTF@SiO_2 or SiO_2 to get the composites **1** and **2**, respectively, that were then stored at room temperature, under a dry air atmosphere. The quantitative deposition of Pt NPs on the supports was verified by ICP-OES analysis, which gave a final Pt content of 2.0 wt.% for both **1** and **2**.

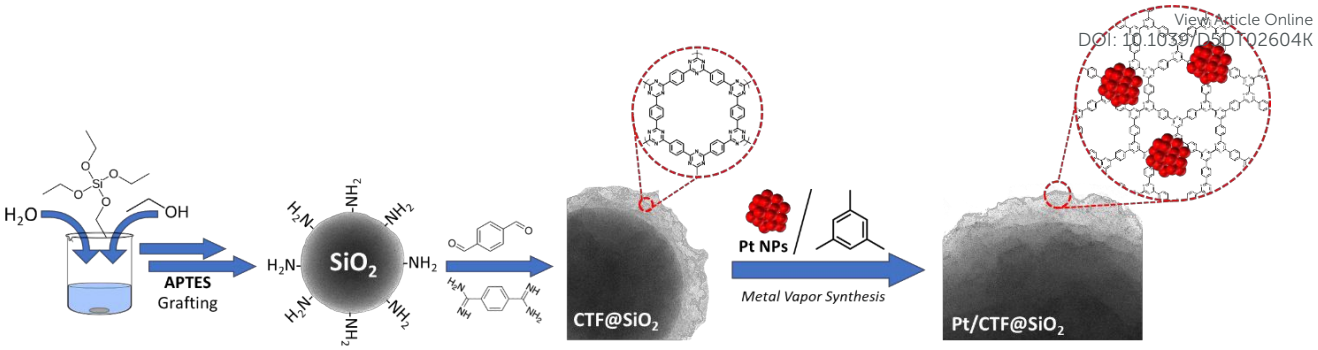

Fig. 1. Synthesis method for **1**.

Transmission electron microscopy analysis was performed to investigate the structural and morphological features of both the pristine supports CTF@SiO_2 and SiO_2 (Figs. 2 a)-c), and Fig. S2, respectively) and of the corresponding derived catalysts **1** and **2** (Figs. 3 and S3, and Fig. S4, respectively). TEM analysis of the CTF@SiO_2 and SiO_2 support showed in both samples the presence of SiO_2 spheres with a very homogeneous size distribution, ranging from 240 to 260 nm in diameter. In addition, CTF@SiO_2 exhibited the additional presence of a rough organic shell (CTF) 25 to 30 nm thick covering the entire surface of the SiO_2 spheres. HAADF-STEM/EDS element map analysis confirmed the presence of both carbon and nitrogen atoms at the outer shell of the CTF-SiO_2 spheres. Interestingly, no formation of segregated organic aggregates outside of the SiO_2 surface was observed. Moreover, FT-IR spectra of CTF@SiO_2 support (Figure 2 d)), as well as of the SiO_2 functionalization intermediates (*i.e.* SiO_2 surface reaction with APTES and the further modification with TPA, Fig S4), confirmed that the growth of the organic framework successfully occurred at the surface of the silica spheres. The obtained CTF@SiO_2 exhibited characteristic vibrations of the triazine units at 1523 and 1367 cm^{-1}, ascribed to C=N stretching vibrations that are identical to that observed for the bare CTF bulk material. Moreover, as expected, the Si-O stretching frequency at 1078 cm^{-1} were observed in the examined samples (Figs. 2 d) and S1).

View Article Online
DOI: 10.1039/D5DT02604K

To get further insight in the structural features of CTF@SiO_2 X-ray Photoelectron Spectroscopic (XPS) analyses were carried out (Figs. 2 e and S5). Survey spectra of the support showed the presence of the expected element composition (*i.e*. Si, C, N and O). High-resolution N1*s* XPS spectra reported in Fig. 2 e), revealed a main component centred at a binding energy (B.E.) of 399.0 eV, which proves the presence of pyridinic nitrogen (C=N−C) stemming from the CTF triazine moieties. In addition, a second N1*s* photoelectron contribution at B.E. of 400.7eV and a shakeup component B.E. of 402.5 eV confirmed also the presence of oxidized nitrogen atoms in the CTF framework.[30-32] The Si2*p* photoelectron spectrum of both supports was characterized by a single contribution at B.E: of ca. 103.7 eV, which corroborated the presence of SiO_2.[33] While bare SiO_2 microspheres exhibited a specific surface area (SSA) of 16 m^2/g, the presence of CTF on the surface of the SiO_2 spheres (CTF@SiO_2) significantly increased the SSA to 33 m^2/g (Table S2). Very low porosity was observed for both materials (Fig. S6) and the H3 type hysteresis loop indicates slit-shaped pores, which are typical of aggregates of plate-like particles.

TEM analysis of both MVS-derived **1** (Figs. 3 a and b), and Fig. S3) and **2** (Fig. S4) showed no appreciable alterations in the structural and morphological properties of the corresponding pristine supports. TEM analysis at high magnifications along with HAADF-STEM/EDS platinum maps showed the presence of highly dispersed Pt-NPs along the support surface, falling in the sub-nanometer range (< 1.3 nm) for both 1 and 2 (Fig. 3b) and S3, and S4, respectively). Similar results were previously reported by depositing pre-formed MVS-derived Pt/mesitylene NPs on different carbon-based supports.[19,29]

View Article Online
DOI: 10.1039/D5DT02604K

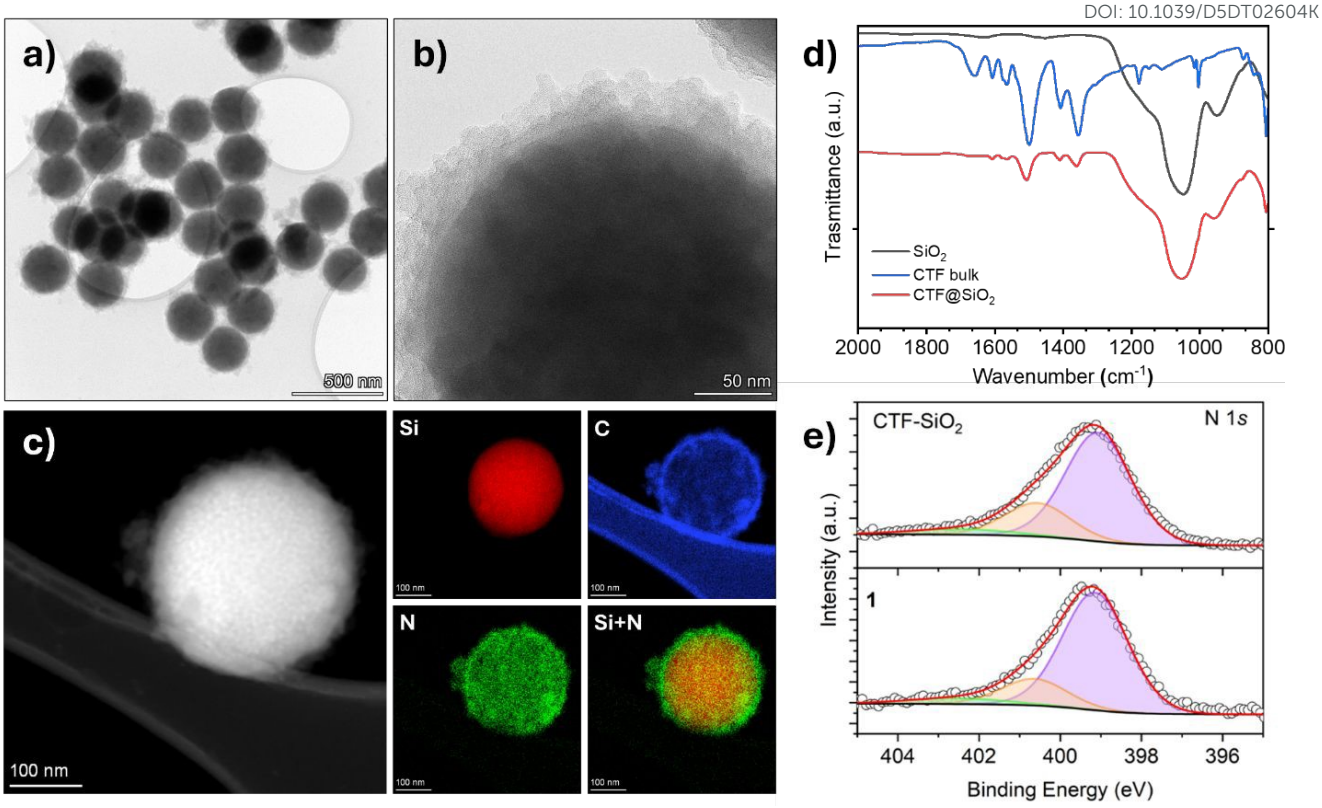

Fig. 2. Representative TEM micrographs of CTF@SiO_2 acquired at low and high magnification, a) and b), respectively; HAADF-STEM/EDS element map, c); FT-IR spectra of SiO_2, CTF and CTF@SiO_2 , d); High resolution N1*s* XPS spectra for CTF@SiO_2, (upper part) and **1** (lower part), e).

The FT-IR spectrum of **1** (Fig. 3 c)) resulted very similar to that registered for pristine CTF@SiO_2, which is indicating the absence of any significant support modification during the immobilization of Pt NPs onto CTF-SiO_2.

XPS analysis of **1** showed the presence of the expected element composition (*i.e.* Si, C, N, O and Pt) (Fig. S7) and the corresponding N1*s* photoelectron spectrum (Figure 2 e)) showed the same feature as that found for CFT@SiO_2. In addition, the B.E. for the pyridinic nitrogen atom at B.E. of 399.1 eV is almost identical to that found for CTF@SiO_2 (399.0 eV), indicating that no Pt–N interaction was detected between the surface Pt and nitrogen atoms of CTF, likely due to the low Pt loading (2 wt.% Pt, see Section 2.2). Interestingly, the Si2*p* photoelectron peak of **1** and **2** exhibited the same

View Article Online
DOI: 10.1039/D5DT02604K

characteristic B.E. of 103.7 eV but notably differed in intensity, which is a clear hint for the presence of the CTF layer entirely covering the SiO_2 nanospheres (Fig. 87). Pt4*f* XPS spectrum shown for **1** in Fig. 3 d) contains two contributions which correspond to Pt(II), which is the major fraction (83.3 at.%), at B.E. of 72.3 eV (Pt4$f_{7/2}$) and Pt(0) at B.E. of 71.1 eV (Pt4$f_{7/2}$).[34,35] Interestingly, the Pt4*f* photoelectron spectrum of **2** is characterized by the presence of a lower percentage of surface Pt(II) atoms (*i.e.* 68.5 at%, Table S1), which might hint to an easier oxidation of surface Pt atoms in **1** due to electron donation originating from CTF nitrogen atoms, compared to **2** (*i.e.* Pt(II) 68.5 at%, Table S1, Fig. S9).

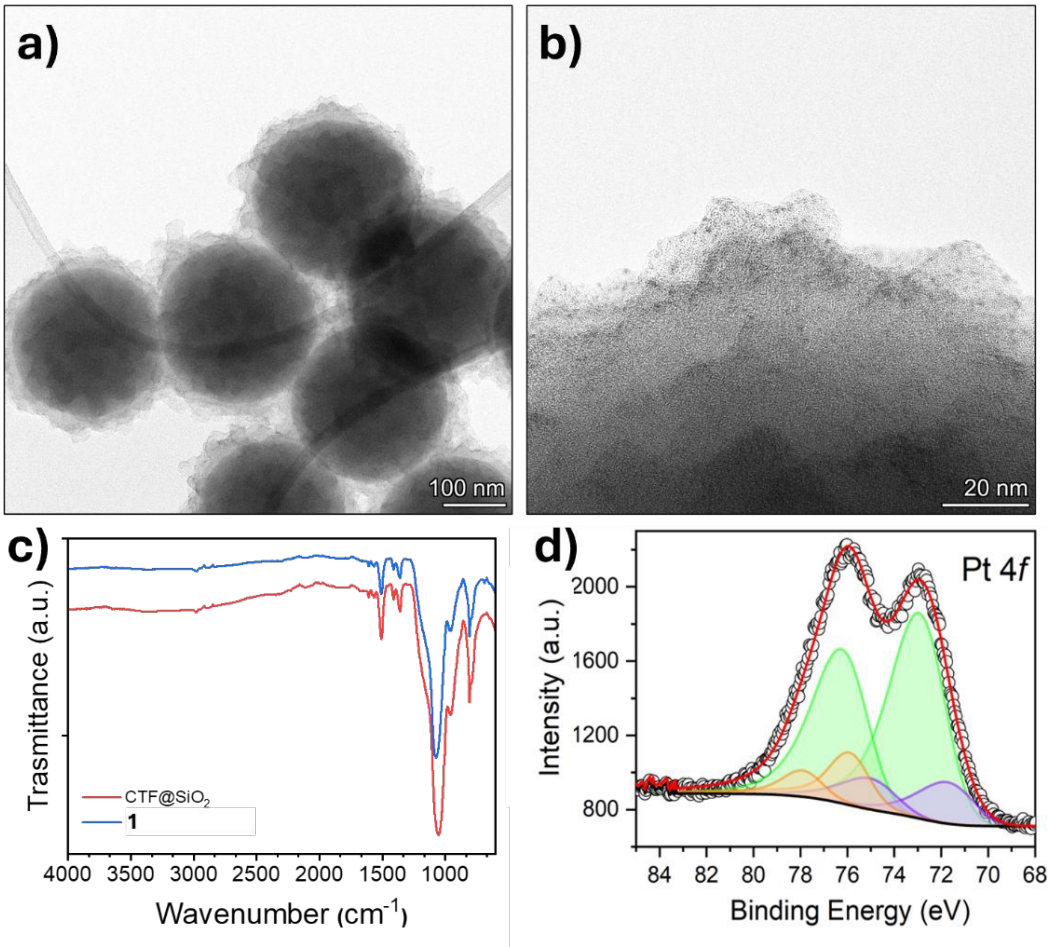

Fig. 3. Structural characterization of **1**: representative TEM micrographs acquired at low, a), and high magnification, b), respectively; FT-IR spectra, c); high resolution XPS spectra in the Pt4*f* core region showing also the Al2*p* photoelectron peaks (orange peaks) originating from a perforated aluminium foil which covered **1** during drying under reduced pressure, d).

View Article Online
DOI: 10.1039/D5DT02604K

The thermal behaviour of **1** and of the corresponding support was investigated by TGA under nitrogen atmosphere (Fig. 4).

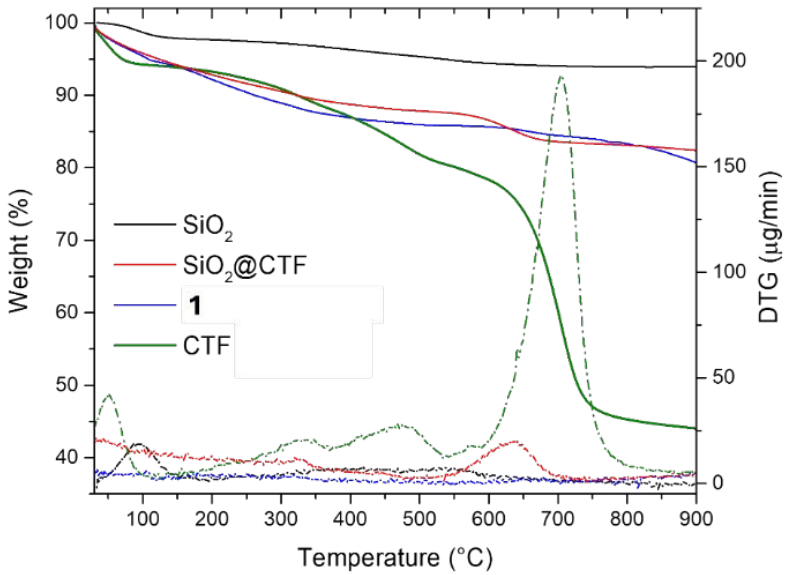

Fig. 4. Thermogravimetric analysis of SiO_2, CTF@SiO_2, **1**, and bulk CTF material.

The TGA curve of pristine silica (SiO_2) showed a minor weight loss of about 6 wt.% up to 900 °C mainly due to the desorption of physically adsorbed water below 150 °C (about 2 %) and to the condensation of surface hydroxyl groups above 200 °C.[36] In contrast, silica coated with the covalent triazine-based framework (CTF@SiO_2) showed an initial weight loss starting around 200 °C and continuing up to 600 °C, followed by a second step between 600 and 900 °C, consistent with the decomposition of the organic framework as observed for the bulk CTF reference. The overall mass loss of this sample (≈18% at 900 °C) corresponds to a CTF content of about 20-25 wt.%. **1** showed a similar decomposition profile to that of CTF@SiO_2, with a slightly higher total weight loss (≈19% at 900 °C), confirming a comparable amount of CTF.

View Article Online
DOI: 10.1039/D5DT02604K

3.2 Catalysis in water

Catalysts **1** and **2** have been screened in water for the hydrogenation of 2,3-BDO and PyA by applying a substrate to Pt molar ratio of 561. The reaction products were analyzed by means of HPLC, ^{1}H NMR spectroscopy and GC-MS spectrometry. All obtained products were quantified by HPLC using calibration curves for each compound. All catalytic reactions were carried twice and the reported results, compiled in Table 1, are average values. To avoid diffusion-controlled reactions, the stirring speed of the autoclave (*i.e*. magnetic stirring) was optimized to 1000 rpm. Also, the hydrogen pressure used in the catalysts' screening (*i.e*. from 5 to 30 bar) was optimized to 25 bar (Table 1). The relatively high hydrogen pressure, needed to obtain a rational conversion of intermediate A into B and C is due to the low solubility of hydrogen in water.[37] In contrast, the conversion of 2,3-BDO in intermediate A occurs at high conversion already at low hydrogen pressure (5 bar) (Table 1).

Irrespective of the catalyst used, the hydrogenation of 2,3-BDO was found to give three reaction products, namely 3,4-dihydroxy-3,4-dimethylhexa-2,5-dione (A), 3-hydroxy-butan-2-one (B) and butane-2,3-diol (C), whereas in the absence of the Pt-based catalyst, no substrate conversion occurred (Table 1, entry 1). Upon carrying out catalytic reactions with either catalyst at two different reaction temperatures (*i.e*. 85 and 105 °C) the stepwise hydrogenation reaction from 2,3-BDO to butane-2,3-diol was obvious.[38-42] At 85 °C 2,3-BDO was converted first into the dimer A, which successively converted into B, as confirmed by catalytic reactions conducted at the latter temperature at different reaction times (Table 1, entries 2, 3 and 9). The chemical nature of dimer A has been proved by ^{1}H and ^{13}C{^{1}H} NMR spectroscopy (Figs. S10, S11) as well as by MS analysis (Fig. S12). This dimer formation contrasts those reported for 2,3-BDO occurring in dichloromethane in the presence of Pt NPs decorated with nitrogen atom containing ligands.[12] The formation of compound A occurred by a reductive coupling of two molecules of 2,3-BDO in the presence of NPs' surface Pt(0) atoms, which action as reducing agent, while water is needed to protonate the deprotonated diol intermediate yielding A (Scheme S1).[43,44] The experimental fact that in the absence of hydrogen 2,3-BDO was not

converted into A, whereas in the presence of a relatively low hydrogen pressure (5 bar) a high 2,3-BDO conversion into A (95%, Table 1, entry 5) was observed, indicates that hydrogen is needed to regenerate Pt(0) NPs' surface atoms.

View Article Online
DOI: 10.1039/D5DT02604K

Table 1. **1** and **2**-catalyzed hydrogenation of 2,3-BDO and PyA in water.

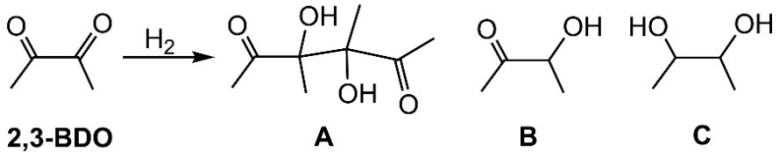

2,3-BDO **A** **B** **C**

Entry[a]	Catalyst	t(h)	T(°C)	Conv. Substrate (%)	A (%)[b]	B (%)	C (%) [*meso*/*rac*]	D (%)	E (%)	F (%)	G (%)
1	-	1	85	-	-	-	-				
2	**1**	0.5	85	93.1	65.9	33.6	0.5				
3	**1**	1	85	96.5	52.2	45.9	1.9				
4[c]	**1**	1	85	-	-	-	-				
5[d]	**1**	1	85	95.0	75.2	24.8	-				
6[e]	**1**	1	85	97.0	68.2	31.8	-				
7[f]	**1**	1	85	98.0	60.0	39.0	1.0				
8[g]	**1**	1	85	97.5	51.0	47.9	1.1				
9	**1**	3	85	100.0	35.2	62.6	2.2				
10	**2**	1	85	96.5	76.8	23.2	-				
11	**2**	3	85	99.5	44.5	55.5	-				
12	**1**	3	105	100.0	-	76.8	23.2				
13	**1**	15	105	100.0	-	0.9	99.1/[3/4]				
14	**2**	3	105	100.0	2.1	95.5	2.4				
15	**2**	15	105	100.0	-	80.9	19.1/[3/4]				
16[h]	**2**	3	105	89.0	20.0	79.0	1.0				
17[h]	**1**	3	105	100.0		77.0	23.0				
18[i]	**1**	3	105	100.0		77.3	22.7				
19[j]	**1**	3	105	100.0		77.8	22.2				

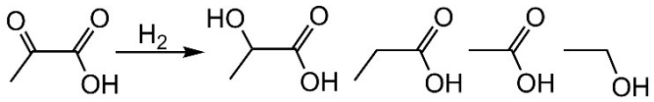

PyA **D** **E** **F** **G**

20	-	1	105	-	-	-	-	-	-	-	-
21[c]	**1**	1	105	-				-	-	-	-
22[f]	**1**	1	105	77.2				92.9	2.2	1.9	3.0
23	**1**	1	105	85.6	-	-	-	90.9	2.9	2.2	4.0
24[g]	**1**	1	105	86.5				89.2	2.9	3.9	4.0
25	**2**	1	105	32.4	-	-	-	83.7	5.5	6.9	3.9
26	**2**	2	105	52.8				91.6	2.9	2.1	3.4
27[h]	**1**	1	105	86.7				90.9	5.9	2.7	0.5
28[i]	**1**	1	105	85.6				90.7	5.5	3.8	-

29[j]	**1**	1	105	85.1		89.9	5.0	5.1

[a] Catalytic condition: Catalyst (20.0 mg, 2.05 μmol of Pt), substrate (1.15 mmol), water (20.0 mL), p(H_2) (25 bar). [b](rac/meso ratio close to 1).[c] Without H_2; [d] p(H_2) (5 bar); [e] p(H_2) (10 bar); [f] p(H_2) (20 bar); [g] p(H_2) (30 bar); [h] 1st recycling. [i] 2nd recycling; [j] 3rd recycling.

At 85 °C only small amounts of C (2.2%) were obtained with the most active catalyst **1** after a reaction time of 3 h (Table 1, entry 9) (Fig. S13). Upon increasing the reaction temperature to 105 °C, a notable conversion of 2,3-BDO into C (23.2%) was obtained for **1** (Table 1, entry 12), while almost quantitative formation of C (99.1%) was gained after a reaction lasting 15 h (Table, entry 13) (Figs. S14, S15). In contrast, **2** led to only 19.1% of C under these latter conditions (Table 1, entry 15 *vs* 13). Irrespective of the catalyst, both stereoisomers of C (*meso*/*rac*) were obtained in a 3:4 molar ratio (Table 1).

The hydrogenation reactions of PyA[45,46] conducted in water at 105 °C and with a hydrogen pressure of 25 bar gave lactic acid (D) as major compound, irrespective of the catalyst used (Figs. S16, S17) (Table 1, entries 20-29). Along with lactic acid, propionic (E) and acetic acid (F) as well as trace amounts of ethanol (G) were formed, when fresh catalysts were used. Propionic acid was obtained from lactic acid by a dehydration/hydrogenation step.[47-51] Acetic acid and ethanol are mainly obtained upon decarboxylation of PyA.[52,53] Analogously to the results obtained in the hydrogenation of 2,3-BDO, **1** showed significantly higher catalytic activity compared to **2** (Table 1, entry 23 *vs* 25) along with a higher lactic acid selectivity (90.9 (**1**) *vs* 83.7 (**2**), due to the formation of lower amounts of propionic and acetic acid.

The significantly higher catalytic hydrogenation activity of **1** compared to **2** is the consequence of efficient surface Pt-N interactions between NPs' surface Pt(0) atoms (Lewis acid sites) and support-nitrogen atoms (Lewis base sites). These Lewis acid-base couples foster the heterolytic hydrogen splitting which leads to the formation of surface Pt-hydride species, which are the real catalytic species, operative in hydrogenation reactions when polar functional groups, such as C=O bonds are intend to convert to the corresponding alcohol functionality.[54]

View Article Online
DOI: 10.1039/D5DT02804K

The stability of both catalysts during hydrogenation reactions in water was verified by carrying out recycling experiments, ICP-OES analyses of the reaction solution after hot filtration, and the structural characterization of the recovered catalysts. As a result, recycling experiments conducted with **1** and **2** under identical catalytic condition proved that **1** gave almost identical substrate conversion for three consecutive catalytic reactions, using 2,3-BDO as substrate (Table 1, entries 17-19), which is in stark contrast to the drop of catalytic activity found for **2**, already after the first recycling experiment (Table 1, entry 16 *vs* 14). In addition, in consecutive catalytic reactions using PyA as substrate, **1** showed also an almost identical conversion with high lactic acid selectivity of roughly 90 % maintained throughout four consecutive catalytic runs (Table 1, entries 23 *vs* 27-29). ICP-OES analyses of the hot filtered solutions gave for both catalysts low leaching, which was close to the detection limit of the instrument (< 2 ppb). TEM analyses of recovered **1** and **2** (*i.e.* after 15 h reaction time at 105 °C (**1**) and after 3 h reaction time at 105 °C (**2**)), are shown in Figs. 5a and b, respectively and confirm the high stability of **1** against sintering (Pt NPs of recovered catalyst showed comparable size respect the as synthesizes one). On the other hand, strong sintering of the Pt NPs was observed in case of **2** (Fig. 5 b)). In agreement with the TEM results, PXRD spectra acquired for recovered **1** and **2**, showed only in case of **2** the presence of the characteristic diffraction peaks assigned to *fcc* Pt (*i.e.* Pt (111) at 39.6 (2Θ) and Pt (200) at 46.4 (2Θ)) (Fig. 5 c)), (Fig. 5 c), trace d; the PXRD pattern of pristine Pt-NPs are shown in Fig 5c, trace e). This experimental result confirms strong sintering of Pt NPs in **2** (*i.e.* average NPs' size of 2.8 nm has been determined by the Debye-Scherrer method [46] based on the Pt(111) Bragg reflex). The TGA curve of recovered **1** (*i.e.* after four catalytic cycles) (Fig. S18) is almost identical to that of as-synthesized **1**, confirming the high stability of the organic CTF phase under real catalytic conditions. The temperature corresponding to the maximum degradation rate (DTG peak) was observed at approximately 700 °C, which is comparable to that of pristine CTF, but shifted relative to the CTF@SiO_2, where the peak appeared around 640 °C. The high stability of SiO_2-supported CTF under the chosen catalytic conditions is

View Article Online
DOI: 10.1039/D5DT02604K

furthermore confirmed by the identity of the FT-IR spectra of recovered **1** (after 3 catalytic cycles) and as-synthesized **1** (Fig. 5 d)).

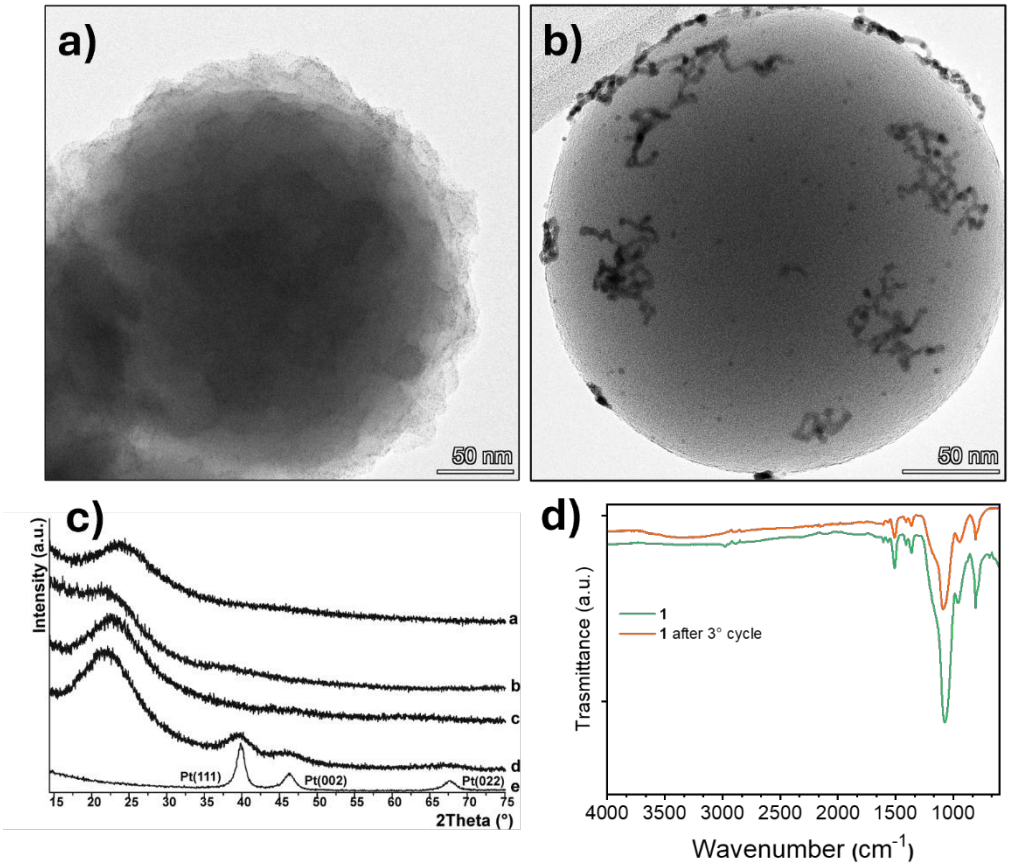

Fig. 5. Representative TEM micrograph of recovered **1** (after 15 h reaction time at 105 °C (a) and recovered **2** (after 3 h reaction time at 105 °C (b)) ; PXRD spectra acquired at room temperature for **1** and **2** (c)): as-synthesized **1** (a); recovered **1** (b); as-synthesized **2** (c) recovered **2** (d) and pristine Pt-NPs (e); FT-IR analysis of as-synthesized **1** (green) and recovered **1** after three catalytic cycles (orange)(Table 1 entry 19).

4. Conclusion

We showed that sub-nanometric-sized Pt NPs (<1.3 nm), synthesized by MVS technique and supported onto a covalent triazine (CTF) framework, which entirely covers SiO_2 nanospheres (**1**), were highly active in the hydrogenation of 2,3-BDO and PyA in water. Butane-2,3-diol and lactic acid were selectively obtained under relatively mild reaction conditions (*i.e.* T, 105 °C and p(H_2), 25 bar). Related catalytic systems hydrogenate 2,3-BDO mainly to 3-hydroxy-2-butanone using ethanol,

View Article Online
DOI: 10.1039/D5DT02604K

toluene, *iso*-propanol or dichloromethane as reaction medium[40-42] and PyA is hydrogenated in water to lactic acid using Ru-based catalysts.[45,54] The crucial role of CTF for the electron donation to surface Pt(0) centers, favouring the formation of Pt-H species which are the dominant catalytic species for C=O bon hydrogenation and stabilizing the Pt-NPs during real catalytic reaction conditions, has been proved by: (*i*) comparing the catalytic activity of Pt NPs onto SiO_2 (**2**) (*i.e*. Pt NPs synthesized by the same method as **1**, showing hence the same Pt dispersion on the support surface) which showed not only a higher catalytic activity for **1**, irrespective of the substrate, but also a higher chemoselectivity mainly in the hydrogenation of PyA to lactic acid (Table 1, < 90%); (*ii*) TEM and PXRD analyses conducted on recovered **1** and **2**, which confirmed in contrast to **1**, **2** experienced a notable NP sintering even after relative short reaction times (3 h); (*iii*) recycling experiments conducted with **1**, which gave almost identical catalytic performance in four successive catalytic reactions, regardless of the substrate used.

5. Acknowledgement

The authors thank the Italian MUR through the PRIN2022 project "HYPOCOF: Hybrid Porous Materials for Eco-sustainable Catalytic Organic Processes" (20222H43S2).

6. References

1 Y. Yusran, H. Li, X. Guan, Q. Fang and S. Qiu, *EnergyChem*, 2020, **2**, 100035.

2 H. El-Kaderi, J. R. Hunt, J. L. Mendoza-Cortez, A. P. Cote, R. E. Taylor, M. O'Keeffe and O. M. Yaghi, *Science*, 2007, **316**, 268-272.

3 S. S. Ahmad Shah, M. S. Javed, T. Najam, M. A. Nazir, A. ur Rehman, A. Rauf, M. Sohail, F. Verpoort and S. J. Bao, *Mater. Today*, 2023, **67**, 229-255.

4 V. Sharma, M. Nemiwal and D. Kumar, *Mini-Rev. Org. Chem.*, 2022, **19**, 815-825.

5 N. Tahir, C. Krishnaraj, K. Leus and P. Van Der Voort, *Polymers*, 2019, **11**, 1326.

6 M. Liu, L. Guo, S. Jin and B. Tan, *J. Mater. Chem. A*, 2019, **7**, 5153-5172.

View Article Online
DOI: 10.1039/D5DT02604K

7 P. Puthiaraj, Y. R. Lee, S. Zhang and W. S. Ahn, *J. Mater. Chem. A*, 2016, **4**, 16288-16311.

8 A. Imehoff, M. Vennewald and R. Palkovits, *Angew. Chem.*, 2023, **62**, e202212015.

9 Y. Li, C. Lai, S. Liu, Y. Fu, L. Qin, M. Xu, D. Ma, X. Zhou, F. Xu, H. Liu, L. Li, Q. Sun and N. Wang, *J. Mater. Chem. A*, 2023, **11**, 2070-2091.

10 D. Ma, X. Huo, C. Lai, H. Yi, L. Zeng, F. Xu, H. Yan, X. Zhou, X. Fan, L. Tang and M. Yan, *Appl. Catal. B: Environ. and Energy*, 2026, **381**, 125894.

11 D. Ma, C. Lai, H. Yi, X. Huo, L. Li, M. Zhang, F. Xu, H. Yan, S. Hu and Y. Luo, *Coord. Chem. Rev.*, 2025, **522**, 216241.

12 X. Zhu, F. Guo, Q. Yang, H. Mi, C. Yang and J. Qui, *J. Power Sources*, 2021, **506**, 230224.

13 M. Gao, G. He, X. Long, S. Wang, Z. Guo, Z. Dong and K. Yuan, *ACS Sustainable Chem. Eng.*, 2024, **12**, 14732-14746.

14 T. He, L. Liu, G. Wu and P. Chen, *J. Mater. Chem. A*, 2015, **3**, 16235-16241.

15 J. Zhang, G. Zhang, L. He, Y. Shi, R. Miao, Y. Zhu and Q. Guan, *Appl. Surf. Sci.*, 2021, **570**, 150881.

16 L. Liao, M. Li, Y. Yin, J. Chen, Q. Zhong, R. Du, S. Liu, Y. He, W. Fu and F. Zheng, *ACS Omega*, 2023, **8**, 4527-4542.

17 H. Vardhan, G. Rummer, A. Deng and S. Ma, *Membranes*, 2023, **13**, 696.

18 E. Pitzalis, R. Psaro and C. Evangelisti, *Inorg. Chim. Acta*, 2022, **533**, 120782.

19 X. T. Nguyen, E. Kitching, T. Slater, E. Pitzalis, J. Filippi, W. Oberhauser and C. Evangelisti, *Catalysts*, 2024, **14**, 798.

20 Y. Bai, H. Feng, N. Liu and X. Zhao, *Energies* 2023, **16**, 5802.

21 M. Dusselier, P. Van Wouwe, A. Dewaele, E. Makshina and B. F. Sels, *Energy Environ. Sci.*, 2013, **6**, 1415-1442.

22 J. A. Slipszenko, S. P. Griffiths, P. Johnston, K. E. Simons, W. A. H. Vermeer and P. B. Wells, *J. Catal.*, 1998, **179**, 267-276.

23 Y. Nagai, S. Morooka, N. Matsubayasi and M. Nakahara, *J. Phys. Chem. A*, 2004, **108**, 11635-11643.

24 D. R. Aireddy and K. Ding, *ACS Catal.*, 2022, **12**, 4707-4723.

25 E. A. Redina, K. V. Vikanova, G. I. Kapustin, I. V. Mishin, O. P. Tkachenko and L. M. Kustov, *Eur. J. Org. Chem.*, 2019, 4159-4170.

26 N. Wang, G. Cheng, L. Guo, B. Tan and S. Jin, *Adv. Funct. Mater.*, 2019, **29**, 1904781.

27 Wang, M. Liu, X. Wang, L. Guo, G. Cheng, C. Zhang, S. Jin, B. Tan andA. Cooper, *Angew. Chem. Int. Ed.* 2017, **56**, 14149.

28 A. J. Barlow, S. Popescu, K. Artyushkova, O. Scott, N. Sano, J. Hedley and P. J. Cumpson, *Carbon*, 2016, **107**, 190-197.

29 W. Oberhauser, C. Evangelisti, R. P. Jumde, R. Psaro, F. Vizza, M. Bevilacqua, J. Filippi, B. F. Machado and P. Serp, *J. Catal.*, 2015, **325**, 111-117.

30 X. Zhu, C. Tian, S. M. Mahurin, S. Chai, C. Wang, S. Brown, G. M. Veith, H. Luo, H. Liu and S. Dai, *J. Am. Chem. Soc.*, 2012, **134**, 10478-10484.

View Article Online
DOI: 10.1039/D5DT02604K

31 Z. Luo, S. Lim, Z. Tian, J. Shang, L. Lai, B. MacDonald, C. Fu, Z. Shen, T. Yu and J. Lin, *J. Mater. Chem.*, 2011, **21**, 8038-8044.

32 A. Mohtasebi, T. Chowdhury, L. H. Hsu, M. C. Biesinger and P. Kruse, *J. Phys. Chem. C*, 2016, **120**, 29248-29263.

33 A. Y. Lee, C. J. Powell, J. M. Gorham, A. Morey, J H. J. Scott and R. J. Hanisch, *Data Sci. J.*, 2024, **23**, 45.

34 M. G. Bancroft, I. Adams, L. L. Coatswirth, D. C. Bennewitz, J. D. Brown and W. D. Westwood, *Anal. Chem.*, 1975, **47**, 586-588.

35 W. Oberhauser, C. Evangelisti, X. T. Nguyen, J. Filippi, L. Poggini, L. Capozzoli, G. Manca, E. A. Kitching, T. J A. Slater and M. Danale, *Inorg. Chem.*, 2024, **63**, 22912-22922.

36 F. Kunc, V. Balhara, Y. Sun, M. Daroszewska, Z. J. Jakubek, M. Hill, A. Brinkmann and L. J. Johnston, *Analyst*, 2019, **144**, 5589-5599.

37 Z. Zhu, Y. Cao, Z. Zheng and D. Chen, *Energies*, 2022, **15**, 5021.

38 H. Duan, Y. Yamada and S. Sato, *Catal. Commun.*, 2017, **99**, 53-56.

39 N. Carrara, J. Badano, N. Bertero, G. Torres, C. Betti, L. Martinez-Bovier, M. Quiroga and C. Vera, *J. Chem. Technol. Biotechnol.*, 2014, **89**, 265-275.

40 N. Carrara, J. M. Badano, F. Coloma-Pascual, C. Vera and M. Quiroga, *Chem. Pap.*, 2017, **71**, 1669-1683.

41 R. P. K. Wells, N. R. McGuire, X. Li, R. L. Jenkins, P. J. Collier, R. Whyman and G. J. Hutchings, *Phys. Chem. Chem. Phys.*, 2002, **4**, 2839-2845.

42 M. Studer, V. Okafor and H.-U. Blaser, *Chem. Comm.*, 1998, 1053-1054.

43 Y.-S. Yang, Z.-L. Shen and T-P. Loh, *Org. Lett.*, 2009, **11**, 2213-2215.

44 B. Cao, S. Li, W. Kong, J. Guo, Z. Tian and G. Zhang, *Inorg. Chem. Commun.*, 2020, **121**, 108227.

45 R. Luque and J. H. Clark, *Catal. Commun.*, 2010, **11**, 928-931.

46 Jones and S. J. Jenkins, *J. Am. Chem. Soc.*, 2008, **130**, 14483-14492.

47 X. Li, J. Pang, J. Zhang, C. Yin, W. Zou, C. Tang and L. Dong, *Ind. Eng. Chem. Res.*, 2019, **58**, 101-109.

48 X. Li, Z. Zhai, C. Tang, L. Sun, Y. Zhang and W. Bai, *RSC Adv.*, 2016, **6**, 62252-62262.

49 Z. Huo, J. Xiao, D. Ren, F. Jin, T. Wang and G. Yao, *Green Chem.*, 2017, **19**, 1308-1314.

50 S. Liu, H. Feng, T. Li, Y. Wang, N. Rong and W. Yang, *Green Chem.*, 2020, **22**, 7468-7475.

51 Y. Nagai, C. Wakai, N. Matubayasi and M. Nakahara, *Chem. Lett.*, 2003, **32**, 310-311.

52 D. R. Aireddy and K. Ding, *ACS Catal.*, 2022, **12**, 4707-4723.

53 U. Holzwarth and N. Gibson, *Nat. Nanotechnol.*, 2011, **6**, 534.

54 W. Oberhauser, L. Poggini, L. Capozzoli, M. V. Pagliaro, S. Coiai and C. Evangelisti, *Inorg. Chem.*, 2025, **64**, 14382–14394.

Consiglio Nazionale delle Ricerche

Istituto di Chimica dei Composti Organometallici (ICCOM)

View Article Online
DOI: 10.1039/D5DT02604K

Dear Editor,

- The data supporting this article have been included as part of the Supplementary Information.

Best personal regards,

Yours sincerely,

Dr. Claudio Evangelisti

Dr. Werner Oberhauser

CNR-ICCOM Sede Secondaria di Pisa
Via G. Moruzzi 1 - 56124 Pisa
Tel. 055 522 5280 (Direttore) – direttore@iccom.cnr.it
Tel. 050 315 2552 (Segreteria PI) – segreteria.pi@iccom.cnr.it
PARTITA IVA N. 02118311006 - CODICE FISCALE N. 80054330586